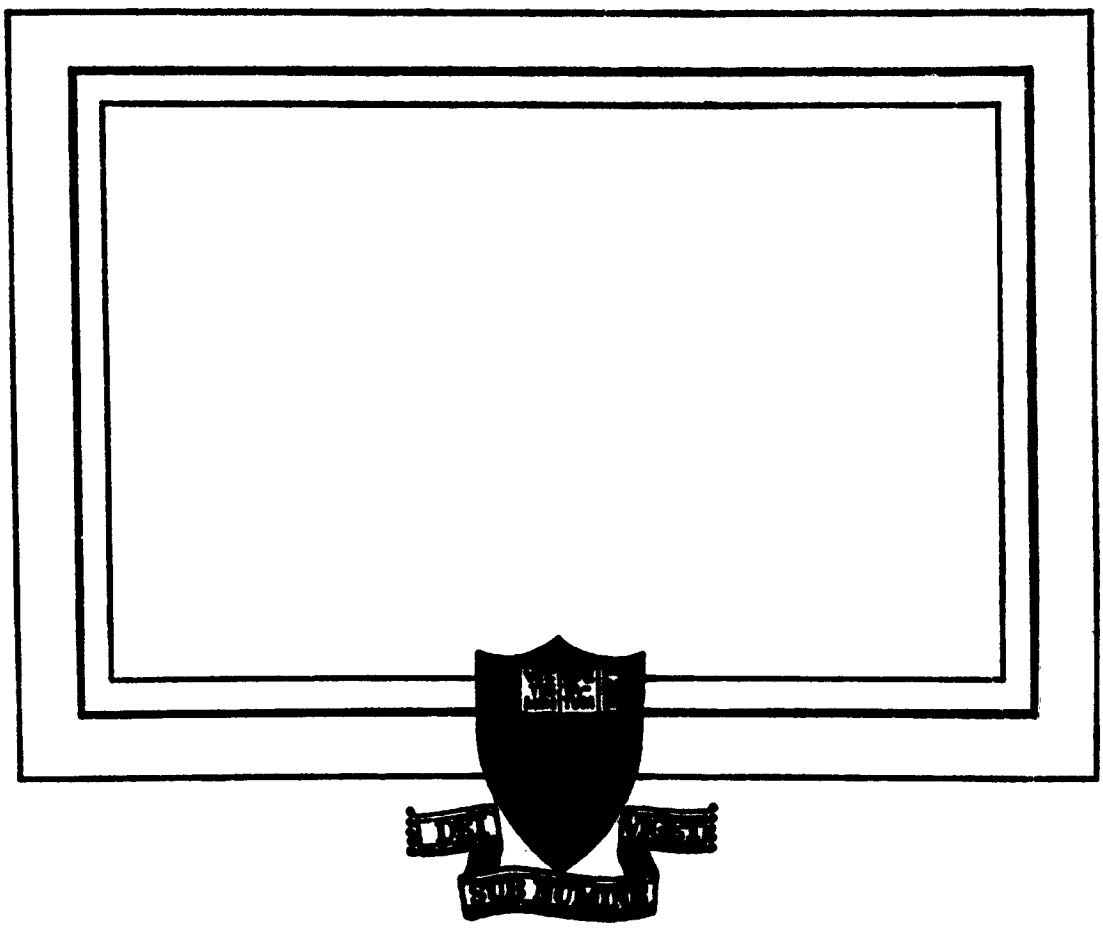



# PRINCETON UNIVERSITY

Princeton University

ONR Contract Nonr 1858(24)

NR-061-041

Technical Report No. 6

# THE STRUCTURE OF SHOCK FRONTS IN ARGON AND NITROGEN

by

M. Linzer and D. F. Hornig

Frick Chemical Laboratory

Princeton University



1 April 1963

# THE STRUCTURE OF SHOCK FRONTS IN ARGON AND NITROGEN*

by

Donald F. Hornig and Melvin Linzer+
Frick Chemical Laboratory
Princeton University, Princeton, N. J.

## Abstract

The optical reflectivity method was used to investigate the structure of shock fronts in argon from Mach 1.70 to Mach 4.85 and in nitrogen from Mach 2.01 to Mach 3.72. Experimental data were obtained at two wavelengths and over a wide range of initial pressures. The reflectivities, corrected empirically for shock curvature, were fitted to a bimodal profile to yield a maximum-slope density thickness. The reciprocal of the thickness in argon (expressed in terms of the Maxwellian mean free path in the undisturbed gas) rises rapidly to a maximum of approximately 0.31 at about Mach 3.5 and decreases gradually thereafter. Above Mach 3 the thickness is about 50% greater than calculated from the Navier-Stokes equations, using a realistic viscosity-temperature relationship. There is excellent agreement, especially at the higher shock strengths, with recent bimodal calculations carried out by Muckenfuss, using realistic intermolecular potentials. In nitrogen, the shocks are thinner than in argon and appear to attain a minimum value of 2.5 initial mean free paths at about Mach 3.7. Rotational relaxation appears to be as rapid in the strong shocks as previously observed in weak shocks; it appears to be completed within the shock front. The experimental density thicknesses are approximately 50% greater than those calculated from the Navier-Stokes equations, using experimental shear viscosity $\mu$ and a bulk viscosity of $2\mu/3$. The agreement with these Navier-Stokes solutions is about as good as those in argon.

---

*The work reported here is based on a thesis submitted by Melvin Linzer in partial fulfillment of the requirements for the degree of Doctor of Philosophy at Princeton University, 1962.

+Present address: National Bureau of Standards, Washington, D. C.

## Introduction

The structure of shock fronts in various gases has been investigated by a number of experimental techniques in the last few years[1-10]. Up to

1. G. R. Cowan and D. F. Hornig, J.Chem.Phys., 17, 1008 (1950). E. F. Greene, G. R. Cowan, and D. F. Hornig, ibid., 19, 427 (1951). W. H. Andersen and D. F. Hornig, Phys. Fluids, 4, 650 (1961).
2. E. F. Greene and D. F. Hornig, J.Chem.Phys., 21, 617 (1953).
3. W. H. Andersen and D. F. Hornig, Mol. Phys., 2, 49 (1959).
4. K. Hansen and D. F. Hornig, J.Chem.Phys., 33, 913 (1960).
5. K. Hansen, D. F. Hornig, B. Levitt, M. Linzer, and B. F. Myers, Rarefied Gas Dynamics, 593, Academic Press, New York (1960).
6. F. S. Sherman, NACA TN 3298 (1955).
7. L. Talbot and F. S. Sherman, Rept. HE-150-137, Univ. of Calif. Inst. of Eng. Res., Berkeley (1956).
8. L. Talbot and F. S. Sherman, NASA Memo 12-14-58w (1959).
9. H. N. Ballard and D. Venable, Phys. Fluids, 1, 225 (1958).
10. R. E. Duff and W. M. Webster, Bull. Am. Phys. Soc., II, 283 (1959).

about Mach 2 no clear cut differences have appeared between the shock thicknesses determined experimentally and those predicted by the Navier-Stokes equations, a surprising result in view of the large deviations from thermal equilibrium which exist within the shock. Indeed, it has been pointed out by Sherman and Talbot[11] that the kinetic theory which leads

11. F. S. Sherman and L. Talbot, Rarefied Gas Dynamics, 161, Pergamon Press, New York (1960).

to the Navier-Stokes equations breaks down completely above Mach 5, giving a physically impossible molecular velocity distribution.

The effect of higher order terms in the kinetic theory has been studied theoretically and leads to the conclusion that above Mach 2 the thickness would deviate substantially from the Navier-Stokes predictions. However, all of these theories suffer from convergence problems in the series solutions. An alternative approach was proposed by Mott-Smith, namely to uses a bimodal velocity distribution, and it has served as a basis for a number of further

studies. The bimodal theory predicts substantially thicker shock fronts than the Navier-Stokes equations, particularly in the region above Mach 2.

The situation, therefore, is that the real differences between the various theoretical approaches develop above Mach 2 where there are very few measurements. Consequently, it seemed important to extend the measurements of shock front thicknesses to shock strengths substantially above Mach 2.

It appeared to us that of the three experimental techniques currently used for studying shock structure, the optical reflectivity method[1-5] had the best chance of success at higher Mach numbers. Although the electron beam technique has been used to investigate shock structure up to Mach 6[10], the results obtained were only of a preliminary nature and were difficult to interpret. As for the free molecule probe method[6-8], the problems involved in producing stationary shock fronts beyond Mach 2 set an upper limit to the range of shock strengths which could be studied.

In order to make optical reflectivity measurements on stronger shocks than heretofore, it was necessary to strengthen the apparatus and to employ much higher driver pressures than in earlier work, since the requirement that the thickness be substantially less than the wavelength of the light employed precluded the lowering of the initial pressure. In many cases combustion driving was employed. We were thus able to generate shock waves as strong as $M = 4.7$ with initial pressures of approximately one atmosphere. Furthermore, increased aperture and better baffling of the optical system significantly increased the signal-to-noise ratio, making it possible to extend the measurements to lower reflectivities. In this way, we were able to make measurements up to Mach 4.70 with greater precision than previously achieved.

Another problem in which we were interested was whether rotational relaxation in a diatomic gas was as rapid in strong shocks, where the final temperature is high, as it has been found to be in weak shocks. The experimental thicknesses for weak shocks can be accounted for satisfactorily if, in addition to the shear viscosity, the gas also has a bulk viscosity. In $N_2$ this bulk viscosity is equivalent to a rotational relaxation time of 5.5 collisions. However, in both $N_2$ and CO the apparent final density was about 5% lower than expected at M = 1.55, implying that in the shock front the "effective" heat capacity was about 93% of the equilibrium value for translation and rotation. More recently, preliminary measurements of the reflectivity of shock fronts in oxygen at Mach 3[5] indicated an even greater discrepancy between the observed and the theoretical equilibrium densities. Since these studies implied that not all of the rotational heat capacity was effective in the shock front region, it was of interest to undertake a more extensive study of translational-rotational energy exchange in a diatomic gas at high temperatures.

## The Optical Reflectivity Method

In the optical reflectivity method a collimated beam of light from an intense high-pressure mercury lamp is reflected off the shock front, passes through a narrow band interference filter, and is brought to a focus on the cathode of a photomultiplier tube. The reflectivity, R, is given by the equation,

$$R = \left[\frac{(\Delta n)^2(1 + \tan^2 \theta)}{4n_1^2}\right] R'(\lambda/\cos \theta) \qquad (1)$$

where $\Delta n$ is the change of index of refraction across the shock front, $\theta$ is the angle of incidence (and reflection) between the light beam and the normal to the shock front, and $\lambda$ is the wavelength of light. $R'(\lambda/\cos\theta)$ is a reduced reflectivity given by the expression,

$$R'(\lambda/\cos\theta) = \frac{1}{(\Delta n)^2} \left| \int_{-\infty}^{+\infty} \left(\frac{dn}{dx}\right) \exp[-i(4\pi \cos\theta/\lambda)x]dx \right|^2 \qquad (2)$$

the integral being the Fourier transform of $(\frac{dn}{dx})$. The shock front density profile used in calculating $R'$ in this work was of the form,

$$\rho(x) = \rho_1 + \frac{\Delta\rho}{1 + \exp(-4x/L)} \qquad (3)$$

where L is the maximum slope thickness. This profile is exact for the bimodal theory of Mott-Smith and approximates all other shock front models closely for low Mach numbers.

$$\Delta n = (n_o - 1)\left(\frac{\rho_1}{\rho_o}\right)\left(\frac{\Delta\rho}{\rho_1}\right) \qquad (4)$$

where the subscript "o" refers to N.T.P., and the index of refraction varies with x, the distance along the shock tube, in exactly the same manner as does the density. The reduced reflectivity thus becomes

$$R' = \left[\frac{\pi^2 L \cos\theta/\lambda}{\sinh(\pi^2 L \cos\theta/\lambda)}\right]^2 \qquad (5)$$

By varying the initial pressure, $p_1$, and by using the relation $L = L_o(\frac{p_o}{p_1})$, where $L_o$ is the thickness at one atmosphere, one may get an experimental curve for $R'$ as a function of $(\lambda p_1/\cos\theta)$. At low values of $R'$, this curve is very steep and enables one to determine $L_o$ with considerable accuracy. At high pressures, $R'$ approaches unity and

R approaches $(\Delta n)^2(1 + \tan^4 \theta)/4n_i^2$. Thus, the density change immediately across the shock front may be directly measured. This, in turn, affords a means of studying whether rotational relaxation processes are completed in the shock front.

## Description of Apparatus

The shock tube was made of 2.76 in. i.d. by 0.120 in. thick stainless-steel tubing and consisted of a 5 1/2 foot long high pressure section and 11 1/4 foot long low pressure section. The high pressure section was sufficiently long to prevent the overtaking of the shock wave by the reflected rarefaction wave when efficient driver gases were used. Because strong shock waves were needed, provisions were made in the high pressure section for combustion driving. A 70% helium, 20% hydrogen and 10% oxygen mixture was used in all combustion-driven shocks. The mixture was ignited by the simultaneous firing of nine spark plugs which were equally spaced along the length of the high pressure section. These were pulsed by the discharge of a condenser bank through automotive spark coils. The apparatus was carefully designed to prevent the occurrence of detonations and considerable attention was paid to the strength requirements of the chamber. Initial pressures up to 300 p.s.i.a. in combustion-driven shocks, and up to 1200 p.s.i.a. in hydrogen-driven shocks, were repeatedly used without any mishaps. The shocks were initiated by the spontaneous rupture of scribed aluminum diaphragms, separating the two sections of the tube. Because of the extreme care taken in scribing the diaphragms, remarkable reproducibility in bursting pressure was obtained. The mean deviation in shock speed in about 80% of the experiments was less than 0.5% and was almost never greater than 1%.

Shock wave velocities were measured by means of light screens. The technique employed differed from the more conventional one[12] in that

12. J. Emrich, Tech. Rept. II - 2NR 061-021, Princeton Univ.(1948); W. Bleakney, High Speed Aerodynamics and Jet Propulsion, Vol IV, 159, Princeton Univ. Press, Princeton (1954).

light was reflected off the front of the shock wave rather than the back. The pulses from the light screens were fed into a Beckman time-interval meter. The combined timing error resulting from the rise time of the pulses and from the accuracy of the timer was negligible, being of the order of a few tenths of a percent.

A schematic diagram of the optical system employed in the reflectivity measurements is shown in Figure 1. The light source was an Osram HBO 100w/2 high-pressure mercury arc lamp. The entrance beam was collimated by a simple convex lens and its area was defined by a rough pair of slits. The beam then passed through a shock tube window which was coated to minimize reflection losses. The reflected beam traversed a similar window and then a set of accurate slits which served to define the area of the front from which reflected light was accepted. For perfectly parallel light, this area was 9 mm high and 50 mm wide (at $\theta = 82°$), the vertical edges on each side being only 9.5 mm away from the corresponding shock tube windows. The effective width of the beam was much smaller, however, since only the central portion was very intense. The exit slits were followed by a Baird-Atomic narrow-band interference filter centered at either 435 mμ or 579 mμ. Each of the filters had a 7 mμ bandwidth and a peak transmission of about 70%. Transmission at other wavelengths was less than 0.1% of the peak values.

After passing through either of these filters, the beam was focused on the "$\Delta\theta$" slit. This slit was an approximately circular aperture and determined the angular dispersion of the light seen by the 931A photomultiplier tube mounted immediately behind it.

All the optical components were centered about a horizontal axis parallel to the plane of the shock. In order to eliminate errors arising from linear attenuation of shock strength and to minimize errors due to non-linear attenuation, the optical axis was chosen so as to make the point of maximum reflection coincide with the midpoint of the velocity interval for an angle of 82°. Since the light screen shock detection method was also based on reflection off the front of the wave, this arrangement consisted in effect of three velocity stations spaced at equal intervals. The peak of the reflectivity pulse always coincided, to within the combined accuracy of the Beckman timer and oscilloscope time scale, with the midpoint of the larger velocity interval. This indicated that no significant attenuation of shock strength occurred between the two light screen stations.

The output pulse of the photomultiplier tube was taken through a White cathode follower and fed into a Tektronix type 545 oscilloscope. The signal-to-noise ratio was usually more than twenty. The noise arose almost entirely from extraneous light reaching the photomultiplier tube. For Mach numbers above 5, an additional "noise" appeared as a result of the gas behind the shock front becoming luminous at the high temperatures generated by such strong shocks (e.g. about 4000°K at $M = 5$). At low initial pressures, the luminous background was sufficient to mask the reflectivity pulse and it became necessary to increase the pressure in order to obtain adequate reflection-to-luminosity ratios.

The low pressure section of the shock tube was evacuated to 100 microns or less before gases were admitted. The leak rate was negligible in view of the high initial pressures employed. The gases used were taken from commercial cylinders without any further purification. Pressures below an atmosphere were measured on a mercury manometer and above an atmosphere by a 16 in. Heise 0-75 p.s.i. gage which was accurate to within 0.1%.

## The Experimental Procedure and Method of Calculation

In all the experiments reported here, $\lambda$ was either 4350 $\mathring{A}$ or 5790 $\mathring{A}$, and $\theta$, with one exception, was 82°. In any particular group of experiments, the wavelength and the initial pressure were fixed at predetermined values for all the runs, whereas average values were used for the temperature, T, the Mach number, M, and the maximum oscilloscope deflection of the photomultiplier signal, D. D is related to the experimental parameters by the expression

$$D = kR = k\left(\frac{1 + \tan^4 \theta}{4n_1^2}\right)(\Delta n)^2 R'^2 \left(\frac{\lambda p_1}{\cos \theta}\right) \quad , \qquad (6)$$

where k is a constant which depends on the intensity of the incident beam, the transmission coefficient of the optical system, and the sensitivities of the oscilloscope and photomultiplier circuits.

The constant k could be determined by making use of the fact that when $\lambda p_1/\cos \theta$ is great enough, $R' = 1$. Consequently, it was measured by determining the deflections observed from Mach 1.40 shocks in argon at an initial pressure of 60 p.s.i.a. Under these circumstances, using values of $L_o$ determined by previous investigators, R' was 0.93 and 0.96 for wavelengths of 4350 $\mathring{A}$ and 5790 $\mathring{A}$ respectively. Moreover, R' was so high that it was insensitive to errors in the value of $L_o$ assumed.

In early measurements, this value of k was used to calculate the average absolute value of $R'$ for a set of experiments from Equation (6), and $L_o$ was then determined from Equation (5). If $R'$ was much less than unity this method should have yielded accurate values of $L_o$, since $R'$ is then very sensitive to $L_o$. However, it was found that the apparent value of the thickness, $L_o$, differed for shocks at the same Mach number but different initial pressures. It was thus apparent that k was <u>not</u> a constant but depended on the initial pressure, $p_1$, the shock strength, M, or both. To cope with this problem, reflectivity measurements were made at a number of values of$(\lambda\ p_1/\cos\theta)$, and hence $R'$, each set being calibrated against shocks in argon at $M = 1.4$ and $p_1 = 60$ p.s.i.a. The resulting data, as can be seen from the curves in Fig. 2, could be fitted to a theoretical curve of the form of Equation (5) to within the experimental error. However, instead of approaching the asymptote, $R' = 1$, they approached a value $g < 1$. Hence, they acted as if Eq. (5) were correct but the true calibration constant were gk, where g is a function of the shock strength but not of $p_1$. The dependence of g on the Mach number is shown in Fig. 3. The problems this raises will be discussed at greater length later.

For several shock strengths, measurements were carried out in argon at only one value of the parameter $(\lambda p_1/\cos\theta)$. For these cases, g was obtained by interpolation from those experiments in which it was determined by the aforementioned procedure (i.e. from Fig. 3). The calibration constant was then taken as gk to obtain $R'$ from Eq. (6) and $L_o$ from Eq. (5).

## Results

A summary of the pertinent data and results for the individual sets of experiments in argon and nitrogen is given in Table 1. The error

limits shown for $gR'$ are the 90% confidence levels for the mean of this quantity. With the two exceptions indicated in the table, all the reflectivity measurements were made at an angle of incidence of 82° and at a horizontal slit width of 6.96 mm.

Experimental points obtained at approximately the same shock strength, but at different values of the parameter $(\frac{\lambda p_1}{\cos\theta})$, are fitted to the theoretical reflectivity curve as shown in figure 2. Tables 2a (argon) and 3 (nitrogen) give the values of g and $L_o$ determined from these plots. The latter quantity is given in the reduced form, $(\frac{l_1}{L})$, where $l_1 = \frac{16}{5} \frac{\mu}{n\sqrt{2\pi mkT}}$ is the Maxwellian mean-free-path ahead of the shock. It should also be noted that the g factors are normalized relative to the reference value at Mach 1.4 which is set equal to unity.

Whereas Figure 3 shows g is a relatively smooth function of M, there is no correlation with $p_1$, of which it might also have been a function. g factors corresponding to the Mach numbers at which only one value of $(\frac{\lambda p_1}{\cos\theta})$ was investigated were obtained by interpolation from a smooth curve drawn through the points on the argon plot. Results for these experiments are given in Table 2b. Since the highest shock strength at which g was determined experimentally was Mach 4.72, a linearly extrapolated value of g was used for the point at Mach 4.85.

Reciprocal shock thicknesses for argon obtained in this investigation are plotted against Mach number in figure 4. Also shown are experimental points determined by other workers as well as the theoretical Navier-Stokes curve for the density thickness and that calculated from the bimodal theory using several intermolecular potentials. Each of the theoretical curves uses potential parameters which duplicate the experimental viscosities up to the temperatures reached in a Mach 3 shock wave. Reciprocal shock front thicknesses listed in Table 2a

are denoted in the figure by open circles and are the most reliable points since they represent the greatest number of experiments. The g factor for each of these points was determined at the same Mach number at which the thickness was measured, whereas for the experiments reported in Table 2b the g factor had to be estimated by means of a graphical interpolation. It can be seen from figure 4, however, that the elimination of either set of points would not change the essential form of the experimental thickness curve.

Finally, results for the experimental shock thicknesses in nitrogen are compared in figure 5 to the Navier-Stokes density thicknesses, with and without a bulk viscosity term. Each of these points is based on measurements at three values of $(\lambda p_1/\cos\theta)$.

The g Factor: Argon

The g factor may be interpreted as the ratio of the actual calibration constant for the experiment to that at Mach 1.4 in argon. From figure 3, it is seen that this ratio differs from unity and is a function of the Mach number.

Such a situation can occur when the sensitivity of the apparatus changes with shock strength. For example, if the electronic rise time were comparable with the rise time of the experiment, the distortion of the photomultiplier signal would increase with shock speed. This particular effect could be neglected in our experiments, however, since the combined rise time of the circuits and of the oscilloscope input leads was of the order of 0.05 μsec whereas the rise time of the reflectivity pulses was always greater than one μsec.

The g factor would also differ from unity if a Mach number dependent property of the shock wave such as the density ratio or the shape of the

density profile differed from that expected. In view of the great precision to which the validity of the Rankine-Hugoniot equations has been directly verified by very many distinctly different experimental techniques[8,9,10,13] it seems most unlikely that $(\Delta\rho/\rho_1)$ could differ

13. W. Bleakney and W. C. Griffith, Am. J. Phys., 22, 594(1954); J. P. Chesik and G. B. Kistiakowsky, J.Chem.Phys., 28, 956(1958); H. T. Knight and D. Venable, Rev. Sci. Instr., 29, 92 (1958).

from the theoretical value. The effect of profile shape cannot be ruled out quite as decisively but are also unlikely to be the source of difficulty. In the first place, the direct measurements of the profile by Talbot and Sherman, using the thin wire probe method, showed that up to Mach 1.8 the profile followed the Navier-Stokes profile. Secondly, it has been shown that the asymmetry which develops in the theoretical Navier-Stokes profile for strong shocks does not affect the reflectivity appreciably[14]. Thirdly, the bimodal theory

14. L. M. Schwartz and D. F. Hornig, "Navier-Stokes Calculations of Argon Shock Wave Structure", Technical Report No. 5, ONR Contract Nonr 1858(24) NR-061-041, Princeton University, March 1963.

concludes that the density profile of Eq. (3) is exact at all shock strengths. Consequently, this would not appear to be the source of the g factor.

The most likely cause which has occured to us is curvature of the shock front. Such curvature would have resulted in a divergence of the initially parallel beam of light so that not all of the reflected beam would pass through the exit aperture. An analysis of the optical system employed indicates that a radius of curvature of the order of a meter or less would make g significantly less than one.

Curvature has indeed been observed in shock tubes. Lin and Fyfe,[15]

15. S. C. Lin and W. I. Fyfe, Phys. Fluids, 4, 238 (1961).

using an ultraviolet absorption technique, measured shock curvatures in air in a 24" shock tube at initial pressures between 0.02 mm Hg and 0.3 mm Hg with shocks ranging from Mach 12 to Mach 22. Duff and Young[16]

16. R. E. Duff and J. L. Young, III, Phys. Fluids, 4, 812 (1961).

measured the curvature of Mach 1.8 to Mach 6.3 shocks in argon at initial pressures of 0.1 mm to 20 mm Hg, using a 1 1/8" shock tube. Both sets of investigators found the curvature to be proportional to $p_1^{-1/2}$ and independent of the Mach number. Lin and Fyfe also argued that the radius of curvature is proportional to $r^{-1/2}$, if r is the radius of the shock tube.

Extrapolation of these results to our conditions predict a radius of curvature of about 27 meters, rather than the value of about one meter required. Furthermore, neither the $p_1^{-1/2}$ pressure dependence or the independence on Mach number is reflected in the behavior of the g factor. All of these factors cast doubt on our interpretation of its origin.

It is essential to note, however, that the measurements were all made at low pressures under conditions where the boundary layer was laminar. At the initial pressures employed in the present work the boundary layer is partially turbulent. de Boer[17] has studied this

17. P. C. T. de Boer, Tech. Note BN-297, Univ. of Md. (1962).

situation theoretically; he predicts that the curvature should increase with Mach number and be almost independent of initial pressure, in agreement with our observations. Moreover, the magnitude of the axial

bulge he predicts is very much greater than that extrapolated from the low pressure data. Another point of interest is his prediction that non-uniformities of the tube walls increase the curvature. He found experimentally that extremely small irregularities in the shock tube surface and in the alignment of the observation windows with the walls of his rectangular shock tube led to an appreciable increase in shock curvature.

An even larger number of irregularities which could contribute to shock wave disturbance were present in the shock tube used in our experiments. Two oval-shaped windows were inserted in our cylindrical shock tube so as to make the long dimension approximately flush with the shock tube wall. As a result, the internal diameter of the tube was decreased by 1.7% at the center of the windows. Furthermore, the small dimension of the window protruded, at the center, almost 1/16 in. past the shock tube wall, a protrusion that did, however, become smaller in successive experiments as a result of continuous erosion by passing shock waves. Still another possible cause of non-uniformity in the fluid flow was the indirect result of the slight collapse of the shock tube wall during heli-arc welding of the window bosses. The section was bored out but an unexpected "chattering" of the boring tool produced some roughness in the wall which was diminished, but did not quite disappear, with subsequent smoothing. Thus, from both theoretical and experimental considerations, the suggestion that the g factor is caused by shock front curvature seems reasonable.

## The g factor: Nitrogen

Using the calibration constant, k, determined with Mach 1.4 shocks in argon and the theoretical values of $\Delta\rho/\rho_1$, for rotationally equilibrated nitrogen, the asymptotic value of R' also approaches a value $g_{N_2}$

which is less than one. In this case the deviation might be ascribed to a difference between the experimental $\Delta\rho$ and the equilibrium value as well as to its source (curvature?) in argon. There is nothing in our experiment which can distinguish the two. However, if it is assumed that the curvature is the same in nitrogen as in argon, so that the g factor from this source is the same in both gases we are led to the following experimental values of $(\rho_2)$ exptl:

| Mach No. | 2.01 | 2.54 | 2.83 | 3.34 | 3.72 |
|---|---|---|---|---|---|
| $\frac{(\rho_2)\ \text{exptl}}{(\rho_2)\ \text{theor.}}$ | 0.93 | 0.90 | 1.01 | 0.93 | 0.98 |

On the average the densities are some 5% below the value for rotational equilibrium. However, we can certainly conclude that $(\rho_2)$exptl. = $(\rho_2)$ theor. to within the combined uncertainty of the curvature assumption and the experimental scatter. In that case we can also conclude that although in the Mach 3.72 shock wave the nitrogen is heated to 1050°K., the gas comes to rotational equilibrium within the shock front transition. In this case rotational relaxation proceeds essentially in parallel with translational relaxation, even when the quantum number of the most energetic quarter of the molecules changes from J = 12 to J = 22.

## The Thickness of Shock Fronts in Argon and Nitrogen

The reciprocal shock thicknesses in argon and nitrogen are shown in Figures 4 and 5. The reciprocal thickness in argon is seen to rise rapidly to a maximum at about Mach 3.5 and to decrease slowly thereafter. The same qualitative behavior is observed for nitrogen although in that case the shock fronts are thinner and the maximum is attained at a higher shock strength.

For comparison we include the Navier-Stokes density thickness for argon calculated by Schwartz.[14] In this calculation he has utilized a viscosity-temperature relationship which fits experimental data for argon up to 1100°K (M=3) and which is theoretically extrapolated to higher temperatures by utilizing a Lennard-Jones intermolecular potential. It is clear that while the Navier-Stokes curve has the correct qualitative behavior it predicts substantially thinner shocks than are found experimentally when $M > 2$. Also shown are the bimodal theory curves of Muckenfuss[18]

18. C. Muckenfuss, Phys. Fluids, 5, 1325 (1962).

for several intermolecular potentials all of which reproduce the experimental viscosity. The bimodal curves are in better agreement with the experimental thicknesses than the Navier-Stokes curve. The reflectivity results are seen to agree best with the exponential-repulsive (exp-rep) model. The scatter in the experimental points and the approximate nature of both the fitting procedures and theoretical calculations, make it difficult to conclude, however, that our results unambiguously confirm the predictions of any one particular intermolecular potential.

In Figure 5, the experimental nitrogen thicknesses are compared with theoretical density thicknesses calculated by Schwartz[19] from the Navier-Stokes

19. L. M. Schwartz, private communication (1963).

equations using experimental shear viscosities and bulk viscosity set at zero and at 2/3 of the shear viscosity. This value of the bulk viscosity corresponds to a rotational relaxation time of 5.5 collisions.

Since the agreement with the Navier-Stokes equations when the bulk viscosity is included is about as good as was obtained with argon, this value of the bulk viscosity must be roughly correct. One cannot go further at this time than to say that up to Mach 3.7 rotational relaxation seems to be completed during the shock compression and that the effect on the structure of the front can be described approximately by a bulk viscosity term.

## Acknowledgment

We are indebted to the Office of Naval Research for their support of this work. One of us (M.L.) would also like to express his appreciation to the National Science Foundation for its assistance in the form of a fellowship. We are grateful to Dr. B. F. Myers, Jr. for his continued interest and many valuable suggestions.

TABLE 1a

Data and Results of Individual Sets of Experiments in Argon

| Mach No. | No. of Expts. | No. of Calib. | $\lambda$, Å | $p_i$ p.s.i.a. | $\frac{\lambda p_i}{\pi^2 p_o \cos\theta} \times 10^6$ | $gR'$ |
|---|---|---|---|---|---|---|
| 1.70 | 14 | 10 | 5790 | 59.7 | 171.24 | .806 ± .073 |
| 1.70 | 15 | 11 | 5790 | 59.7 | 171.24 | .877 ± .092 |
| 1.71 | 15 | 12 | | 28.05 | 60.45 | .795 ± .092 |
| 1.70 | 10 | 6 | | 11.99 | 25.84 | .468 ± .017 |
| 1.92 | 10 | 7 | | 9.20 | 19.83 | .374 ± .017 |
| 2.02 | 12 | 8 | 5790 | 89.68 | 257.24 | .775 ± .040 |
| 2.05 | 15 | 13 | | 19.55 | 42.13 | .640 ± .058 |
| 2.04 | 14 | 10 | | 9.98 | 19.35 | .386 ± .053 |
| 2.02 | 11 | 7 | | 7.20 | 15.52 | .263 ± .013 |
| 2.20 | 11 | 6 | | 7.20 | 15.52 | .292 ± .017 |
| 2.61 | 12 | 6 | 5790 | 33.69 | 96.64 | .634 ± .058 |
| 2.61 | 12 | 12 | | 15.30 | 32.97 | .578 ± .068 |
| 2.61 | 11 | 8 | | 7.20 | 15.52 | .317 ± .018 |
| 2.81 | 10 | 7 | | 7.20 | 15.52 | .338 ± .036 |
| 2.87 | 8 | 6 | | 6.21 | 13.38 | .256 ± .022 |
| 3.13 | 15 | 10 | 5790 | 24.43 | 70.08 | .638 ± .039 |
| 3.07 | 15 | 8 | 5790 | 14.65 | 42.02 | .619 ± .057 |
| 3.14 | 14 | 10 | | 14.97 | 32.26 | .543 ± .061 |
| [1]3.09 | 13 | 14 | | 14.61 | 31.89 | .610 ± .073 |
| [2]3.18 | 9 | 15 | | 16.11 | 19.97 | .389 ± .026 |
| 3.09 | 11 | 6 | | 7.20 | 15.52 | .335 ± .020 |
| 3.11 | 14 | 10 | | 5.79 | 12.48 | .179 ± .014 |
| 3.33 | 10 | 7 | | 6.21 | 13.38 | .284 ± .019 |
| 3.54 | 10 | 8 | 5790 | 23.69 | 67.95 | .585 ± .093 |
| 3.60 | 10 | 8 | | 13.0 | 28.01 | .486 ± .037 |
| 3.56 | 12 | 11 | | 12.74 | 27.45 | .516 ± .052 |
| 3.52 | 8 | 17 | | 7.54 | 16.25 | .356 ± .043 |
| 3.53 | 10 | 6 | | 7.54 | 16.25 | .364 ± .022 |
| 3.64 | 8 | 9 | | 7.54 | 16.25 | .396 ± .055 |

TABLE 1a (continued)

Data and Results of Individual Sets of Experiments in Argon

| Mach No. | No. of Expts. | No. of Calib. | $\lambda$, Å | $p_1$ p.s.i.a. | $\frac{\lambda p_1}{\pi^2 p_o \cos\theta} \times 10^6$ | $gR'$ |
|---|---|---|---|---|---|---|
| 3.72 | 8 | 17 | | 6.21 | 13.38 | .267 ± .033 |
| 3.84 | 13 | 12 | | 6.21 | 13.38 | .220 ± .017 |
| 4.03 | 11 | 6 | 5790 | 12.0 | 34.42 | .470 ± .041 |
| 4.09 | 10 | 7 | 5790 | 7.62 | 21.86 | .344 ± .017 |
| 4.04 | 11 | 8 | | 9.80 | 21.12 | .401 ± .033 |
| 4.07 | 13 | 9 | | 7.62 | 16.42 | .283 ± .027 |
| 4.05 | 10 | 6 | | 6.21 | 13.38 | .231 ± .015 |
| 4.05 | 12 | 14 | | 5.19 | 11.31 | .163 ± .017 |
| 4.26 | 13 | 9 | | 7.43 | 16.01 | .269 ± .023 |
| 4.42 | 9 | 9 | | 7.35 | 15.84 | .283 ± .038 |
| 4.49 | 10 | 8 | | 6.21 | 13.38 | .182 ± .016 |
| 4.68 | 12 | 9 | 5790 | 8.91 | 25.56 | .367 ± .045 |
| 4.73 | 16 | 16 | | 8.91 | 19.20 | .316 ± .039 |
| 4.77 | 12 | 10 | | 7.33 | 15.80 | .195 ± .027 |
| 4.67 | 10 | 6 | | 5.90 | 12.71 | .181 ± .015 |
| 4.73 | 7 | 7 | | 5.43 | 11.70 | .170 ± .018 |
| 4.85 | 7 | 10 | | 6.21 | 13.38 | 0.168 ± .036 |

1. Beam slit width = 2.16 mm

2. $\theta = 76°$

TABLE 1b

Data and Results of Individual Sets of Experiments in Nitrogen

| Mach No. | No. of Expts. | No. of Calib. | $\lambda$, Å | $p_1$ p.s.i.a. | $\frac{\lambda p_1}{\pi^2 p_o \cos\theta} \times 10^6$ | $gR'$ |
|---|---|---|---|---|---|---|
| 2.02 | 12 | 7 | 5790 | 59.52 | 170.7 | 0.607 ± .031 |
| 2.01 | 12 | 10 | | 16.32 | 35.17 | 0.529 ± .042 |
| 2.01 | 10 | 6 | | 8.29 | 17.86 | 0.310 ± .014 |
| 2.54 | 15 | 7 | 5790 | 44.78 | 128.5 | 0.518 ± .057 |
| 2.53 | 15 | 7 | | 21.99 | 47.38 | 0.490 ± .047 |
| 2.55 | 12 | 7 | | 7.62 | 16.42 | 0.340 ± .033 |
| 2.81 | 12 | 7 | 5790 | 29.78 | 85.42 | 0.592 ± .036 |
| 2.86 | 10 | 7 | | 15.49 | 33.38 | 0.550 ± .030 |
| 2.82 | 11 | 7 | | 7.15 | 15.40 | 0.425 ± .025 |
| 3.32 | 14 | 9 | 5790 | 19.44 | 55.76 | 0.460 ± .051 |
| 3.34 | 13 | 8 | | 13.42 | 28.92 | 0.489 ± .063 |
| 3.36 | 10 | 9 | | 5.79 | 12.48 | 0.302 ± .034 |
| 3.73 | 13 | 8 | 5790 | 14.94 | 42.85 | 0.677 ± .050 |
| 3.71 | 19 | 8 | | 9.36 | 20.16 | 0.460 ± .040 |
| 3.71 | 15 | 9 | | 6.15 | 13.26 | 0.352 ± .036 |

TABLE 2a

Summary of Experiments in Argon Conducted at Several Values of ($\lambda\ p_1/\cos\theta$)

| Mach No. | No. of Sets of Expts. at dif. ($\lambda$, $p_1$, $\theta$) | Total No. of Expts. | Total No. of Calib. | g | R' | $(\frac{l_1}{L})$ |
|---|---|---|---|---|---|---|
| 1.70 | 3 | 54 | 39 | 0.871 | 0.537 | 0.196 |
| 2.03 | 4 | 52 | 38 | 0.776 | 0.497<br>0.339 | 0.240 |
| 2.61 | 3 | 35 | 26 | 0.668 | 0.475 | 0.295 |
| 3.11 | 8 | 95 | 78 | 0.684 | 0.569<br>0.489<br>0.262 | 0.282 |
| 3.57 | 3 | 58 | 59 | 0.603 | 0.617 | 0.346 |
| 4.06 | 6 | 67 | 50 | 0.537 | 0.527<br>0.431<br>0.303 | 0.308 |
| 4.72 | 5 | 57 | 50 | 0.484 | 0.402<br>0.373<br>0.351 | 0.306 |

TABLE 2b

Summary of Experiments in Argon Conducted at Single Values of ($\lambda\ p_1/\cos\theta$)

| Mach No. | No. of Expts. | No. of Calib. | $g^1$ | R' | $\frac{l_1}{L}$ |
|---|---|---|---|---|---|
| 1.92 | 10 | 7 | 0.808 | 0.463 | 0.227 |
| 2.20 | 11 | 6 | 0.758 | 0.386 | 0.259 |
| 2.81 | 10 | 7 | 0.680 | 0.498 | 0.308 |
| 2.87 | 8 | 6 | 0.673 | 0.381 | 0.300 |
| 3.33 | 10 | 7 | 0.625 | 0.455 | 0.332 |
| 3.72 | 8 | 17 | 0.585 | 0.456 | 0.333 |
| 3.84 | 13 | 12 | 0.573 | 0.385 | 0.302 |
| 4.26 | 13 | 9 | 0.528 | 0.510 | 0.302 |
| 4.42 | 9 | 9 | 0.513 | 0.552 | 0.328 |
| 4.49 | 10 | 8 | 0.505 | 0.360 | 0.292 |
| 4.85 | 7 | 10 | 0.470 | 0.357 | 0.291 |

[1]Estimate from Figure 3.

TABLE 3

Summary of Experiments in Nitrogen

| Mach No. | No. of Sets of Expts. | Total No. of Expts. | Total No. of Calib. | $\frac{l_1}{L}$ | $g_{N_2}$ | $\frac{g_{N_2}}{*g_{Ar}}$ |
|---|---|---|---|---|---|---|
| 2.01 | 3 | 34 | 23 | 0.231 | 0.626 | 0.790 |
| 2.54 | 3 | 42 | 21 | 0.327 | 0.521 | 0.732 |
| 2.83 | 3 | 33 | 21 | 0.377 | 0.700 | 1.032 |
| 3.34 | 3 | 37 | 26 | 0.385 | 0.507 | 0.811 |
| 3.72 | 3 | 47 | 25 | 0.393 | 0.551 | 0.942 |

*Estimate from Figure 3.

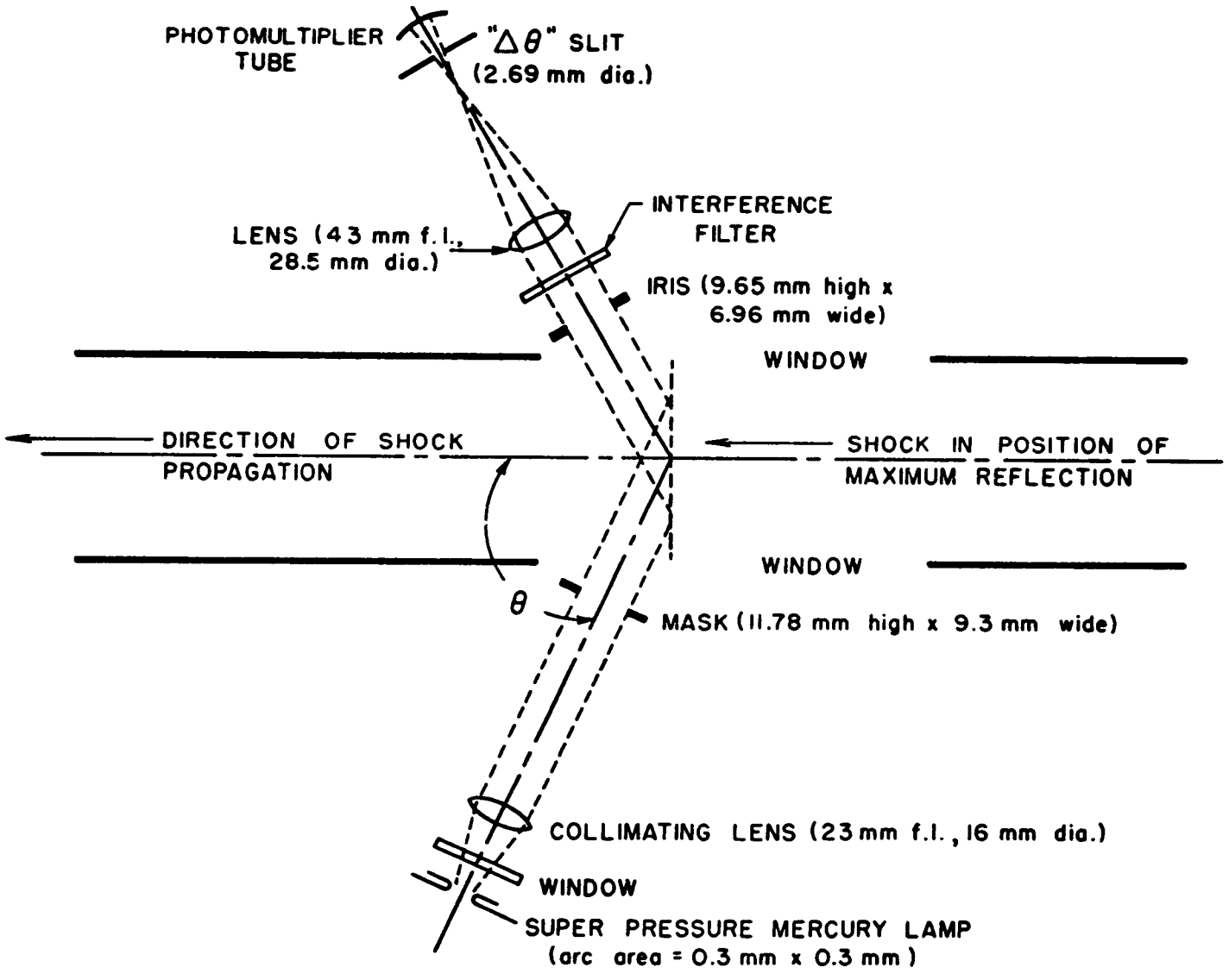


REFLECTIVITY OPTICAL SYSTEM

FIG. 1

Figure 2

Measured Shock Front Reflectivities for Argon. Solid lines are theoretical curves.

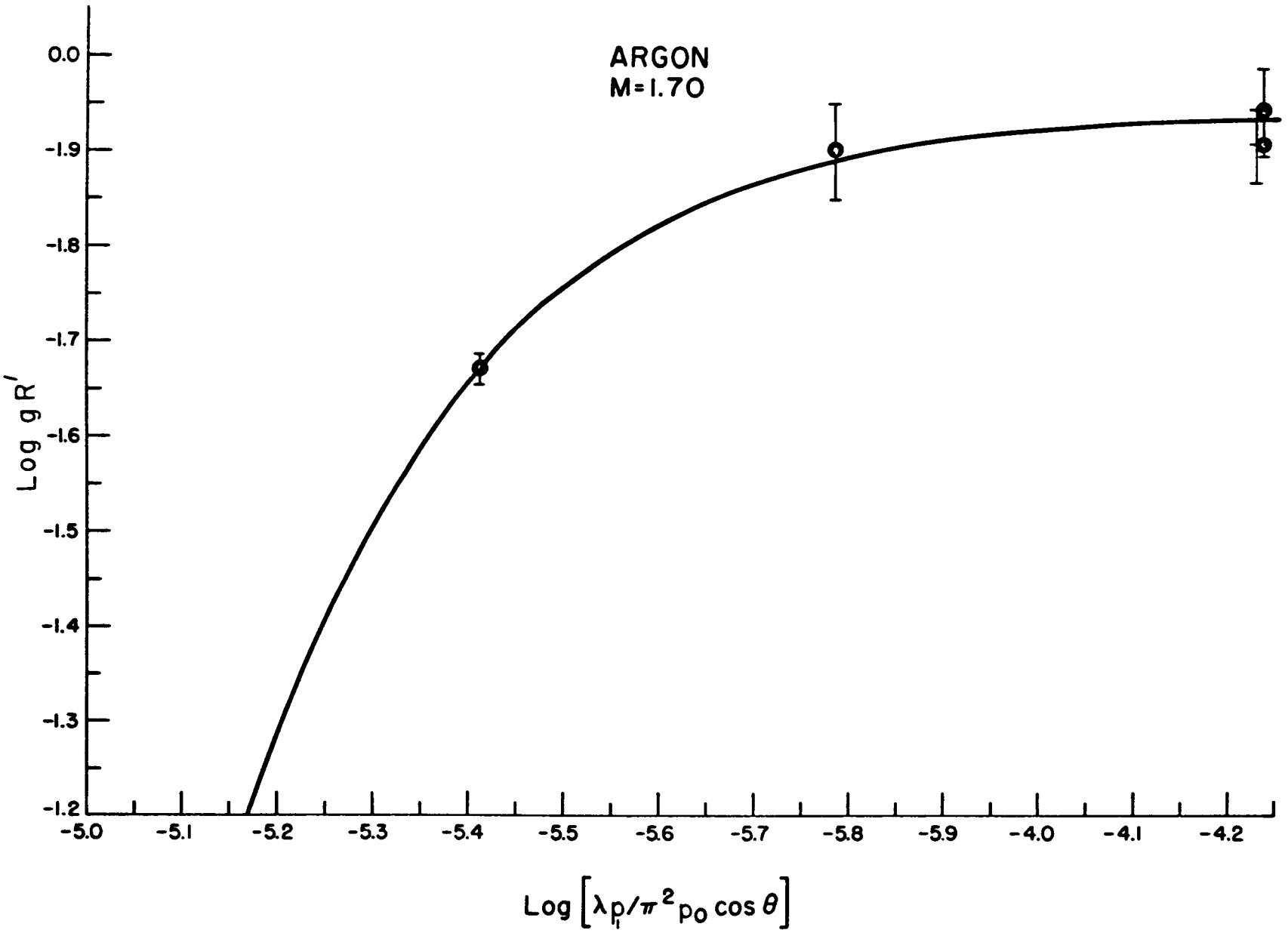
ARGON
M=1.70
0.0
-1.9
-1.8
-1.7
-1.6
-1.5
-1.4
-1.3
-1.2
Log gR'
-5.0
-5.1
-5.2
-5.3
-5.4
-5.5
-5.6
-5.7
-5.8
-5.9
-4.0
-4.1
-4.2
Log [λp_i/π² p_o cos θ]

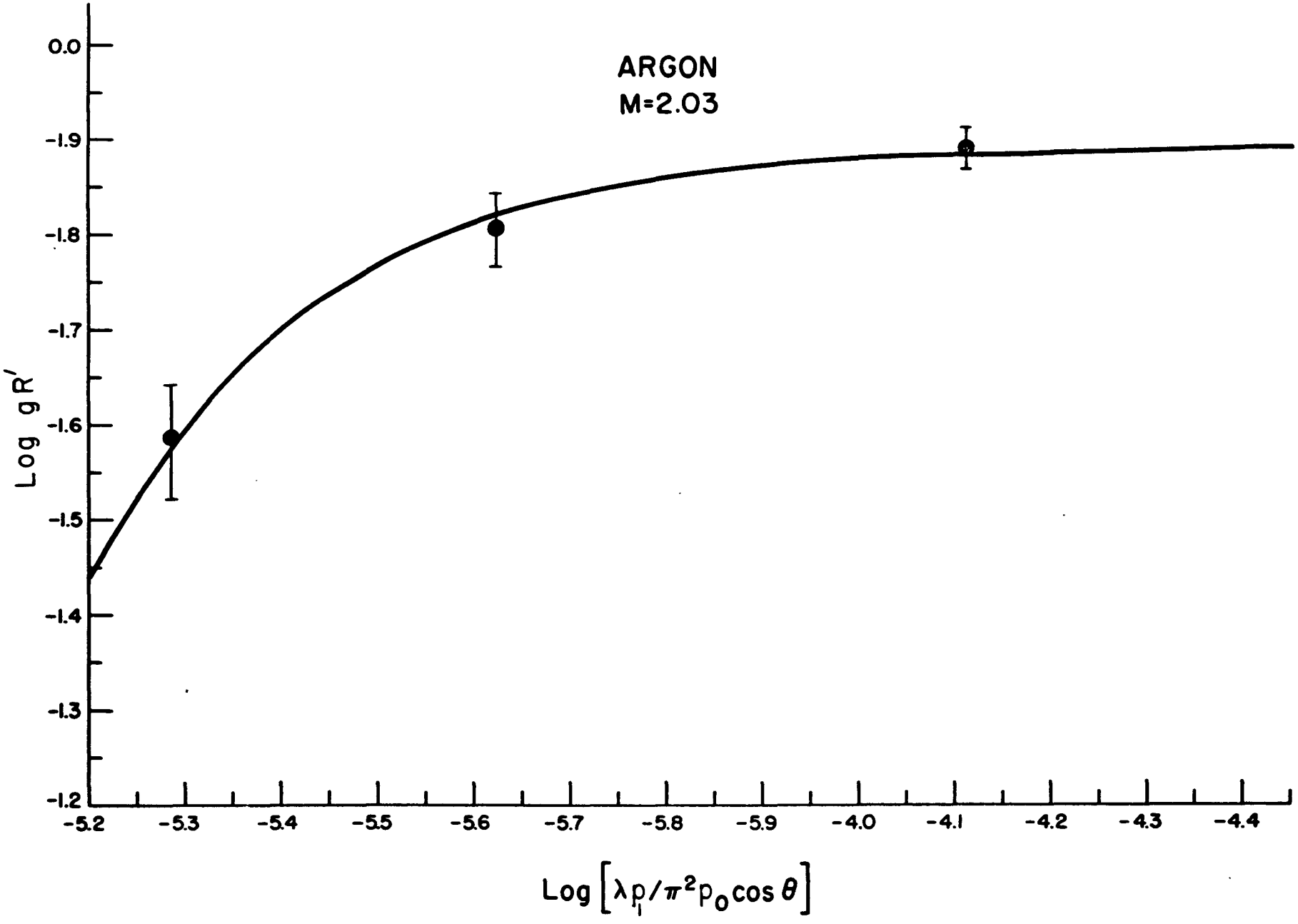
ARGON
M=2.03
0.0
-1.9
-1.8
-1.7
-1.6
-1.5
-1.4
-1.3
-1.2
Log gR'
-5.2
-5.3
-5.4
-5.5
-5.6
-5.7
-5.8
-5.9
-4.0
-4.1
-4.2
-4.3
-4.4
Log [λp_i/π²p_0 cos θ]

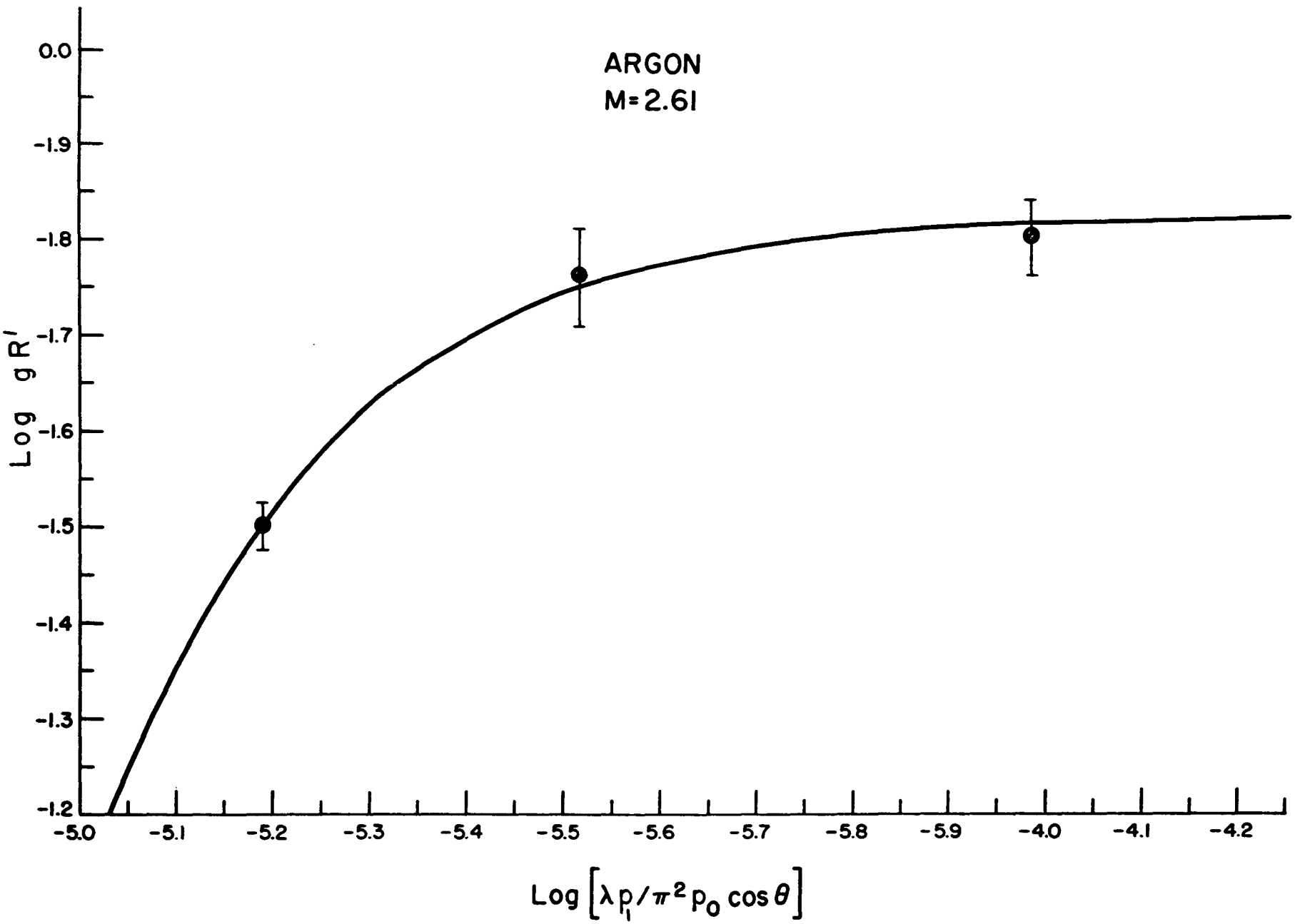
ARGON
M=2.61
0.0
-1.9
-1.8
-1.7
-1.6
-1.5
-1.4
-1.3
-1.2
Log gR'
-5.0
-5.1
-5.2
-5.3
-5.4
-5.5
-5.6
-5.7
-5.8
-5.9
-4.0
-4.1
-4.2
Log [λp/π²p₀ cos θ]

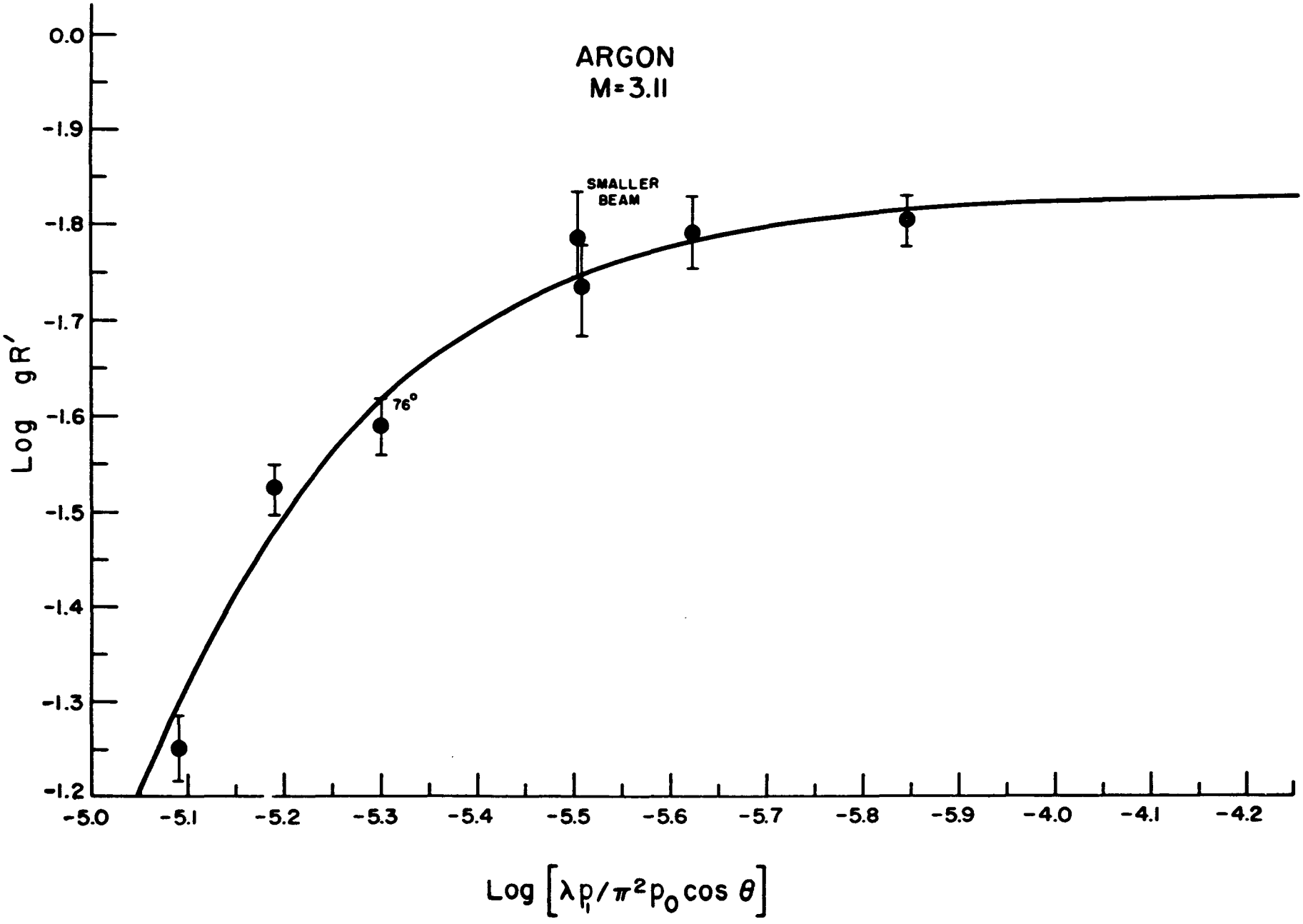
ARGON
M=3.11
SMALLER
BEAM
76°
0.0
-1.9
-1.8
-1.7
-1.6
-1.5
-1.4
-1.3
-1.2
Log gR'
-5.0
-5.1
-5.2
-5.3
-5.4
-5.5
-5.6
-5.7
-5.8
-5.9
-4.0
-4.1
-4.2
Log [λp_1/π²p_0 cos θ]

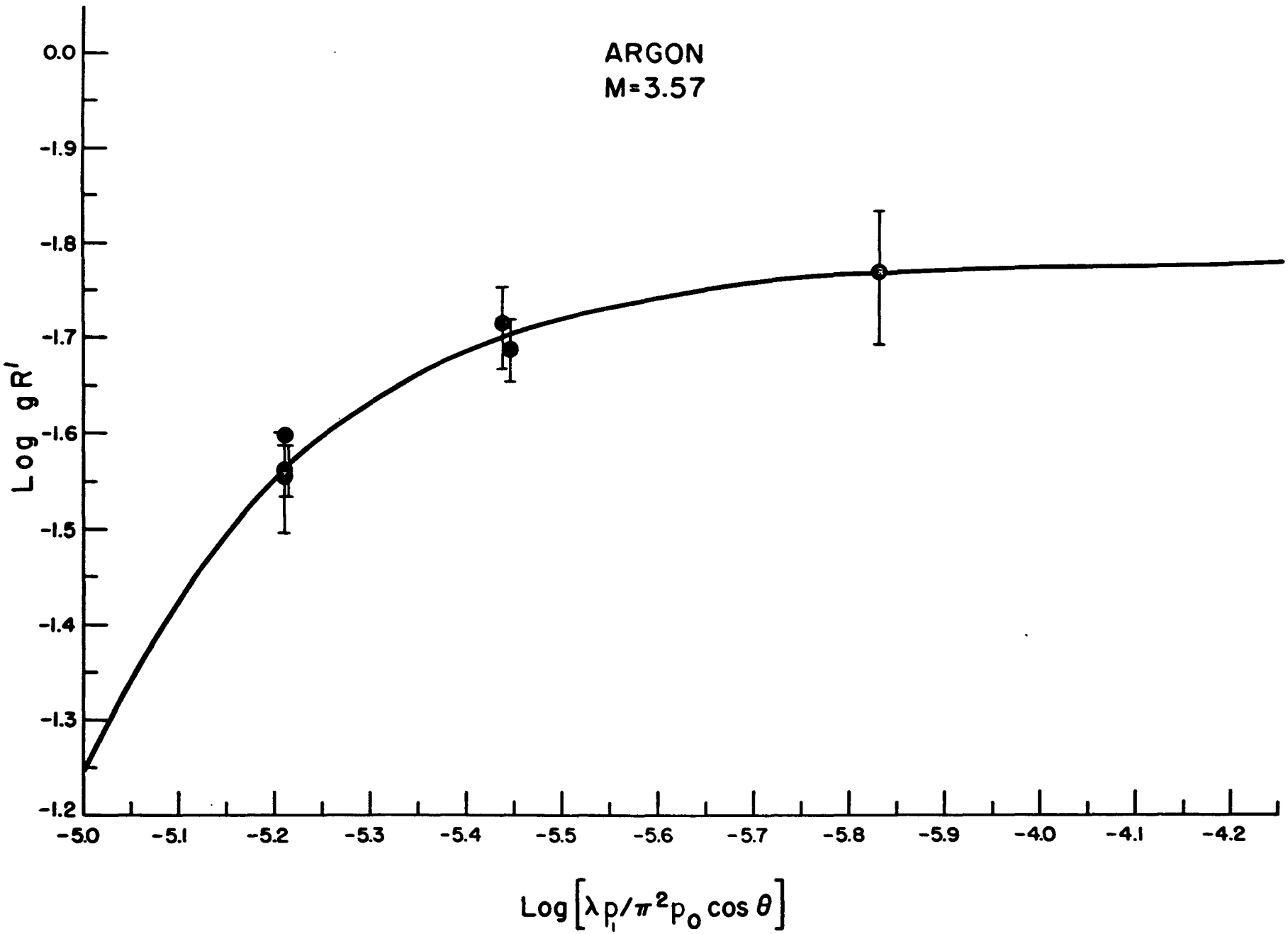
ARGON
M=3.57
0.0
-1.9
-1.8
-1.7
-1.6
-1.5
-1.4
-1.3
-1.2
Log gR'
-5.0
-5.1
-5.2
-5.3
-5.4
-5.5
-5.6
-5.7
-5.8
-5.9
-4.0
-4.1
-4.2
Log [λ p1/π² p0 cos θ]

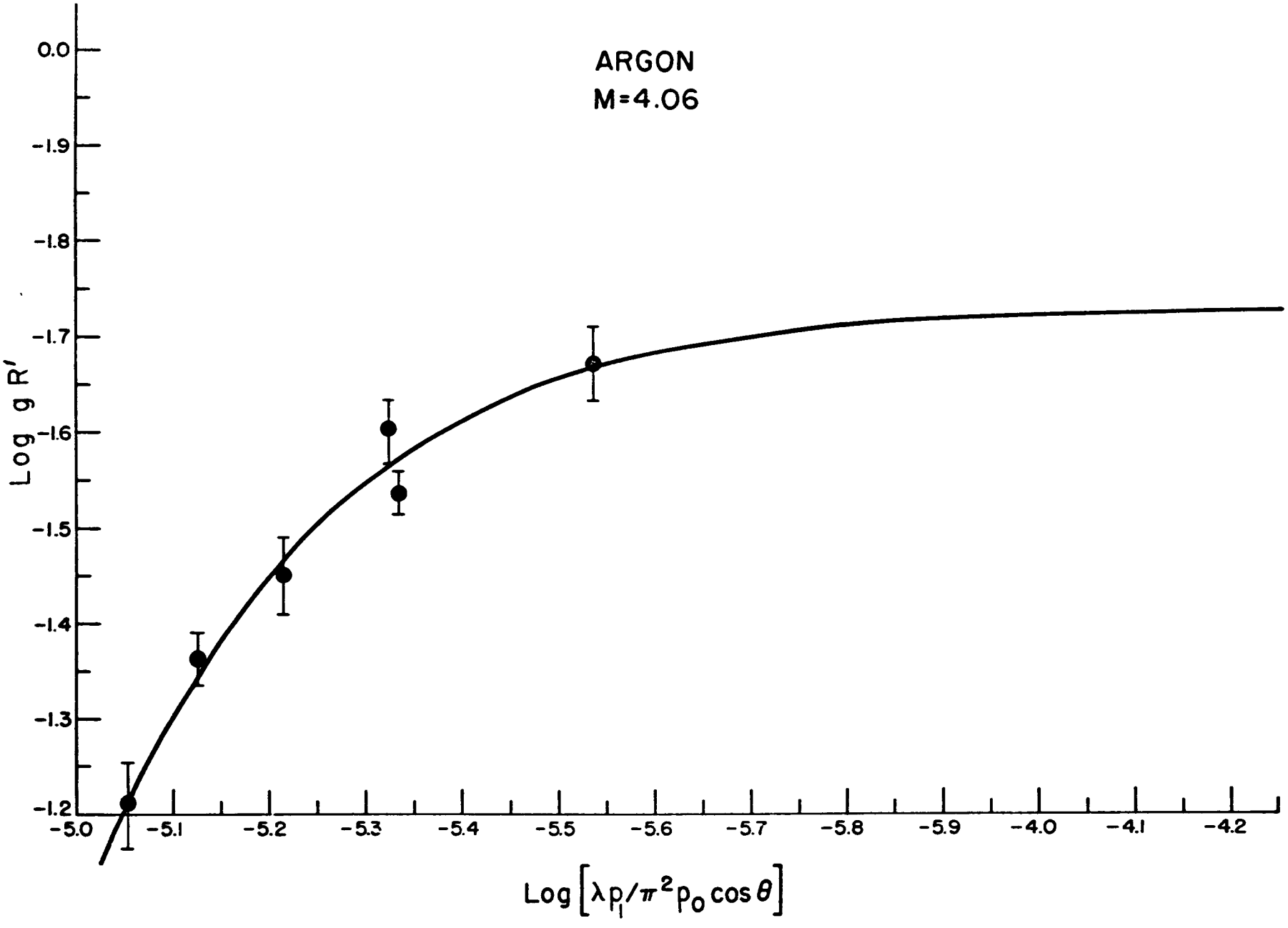
ARGON
M=4.06
0.0
-1.9
-1.8
-1.7
-1.6
-1.5
-1.4
-1.3
-1.2
Log g R'
-5.0
-5.1
-5.2
-5.3
-5.4
-5.5
-5.6
-5.7
-5.8
-5.9
-4.0
-4.1
-4.2
Log [λp₁/π²p₀ cos θ]

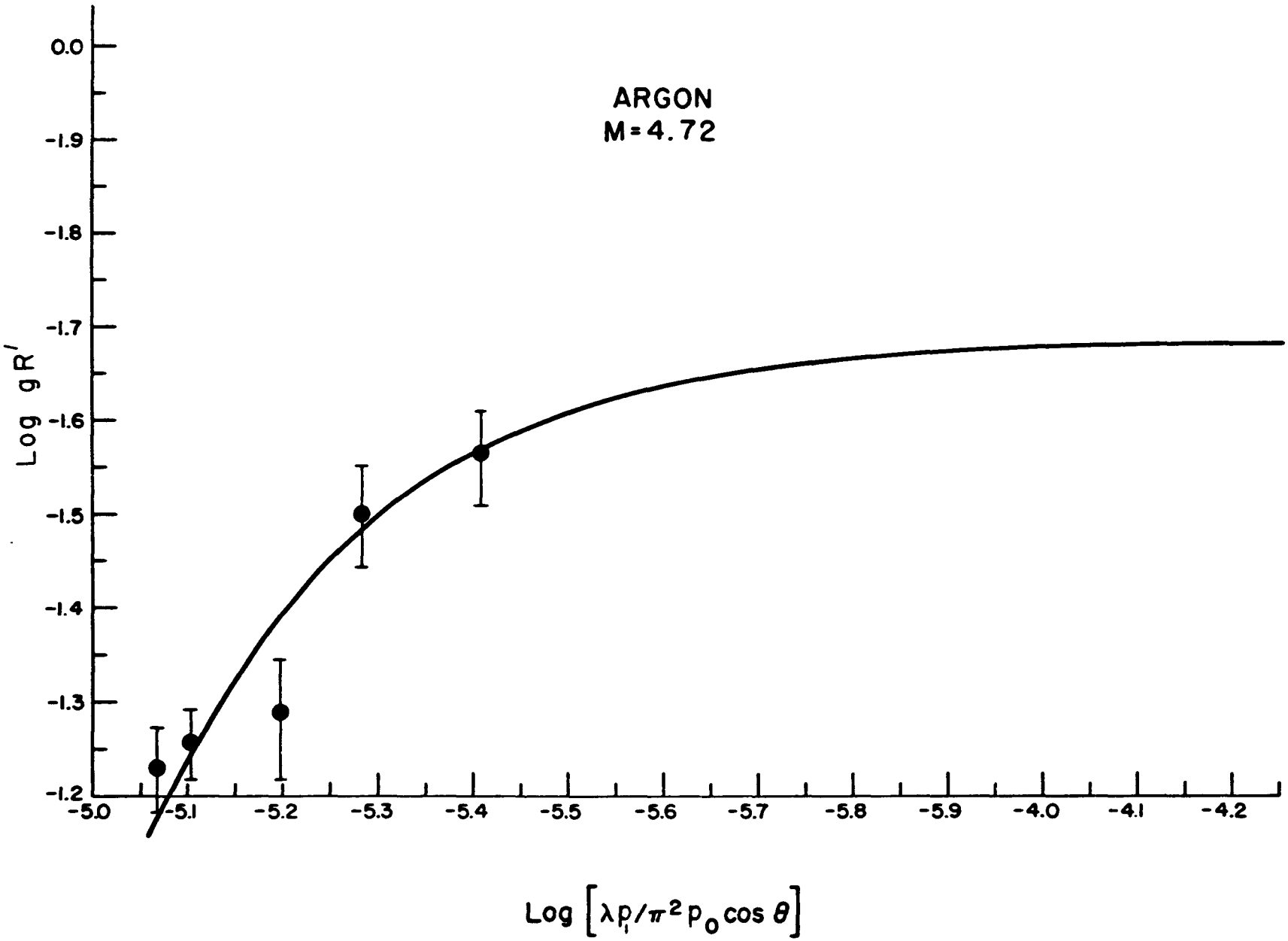
ARGON
M=4.72
0.0
-1.9
-1.8
-1.7
-1.6
-1.5
-1.4
-1.3
-1.2
Log gR'
-5.0
-5.1
-5.2
-5.3
-5.4
-5.5
-5.6
-5.7
-5.8
-5.9
-4.0
-4.1
-4.2
Log [λp_i/π²p_o cos θ]

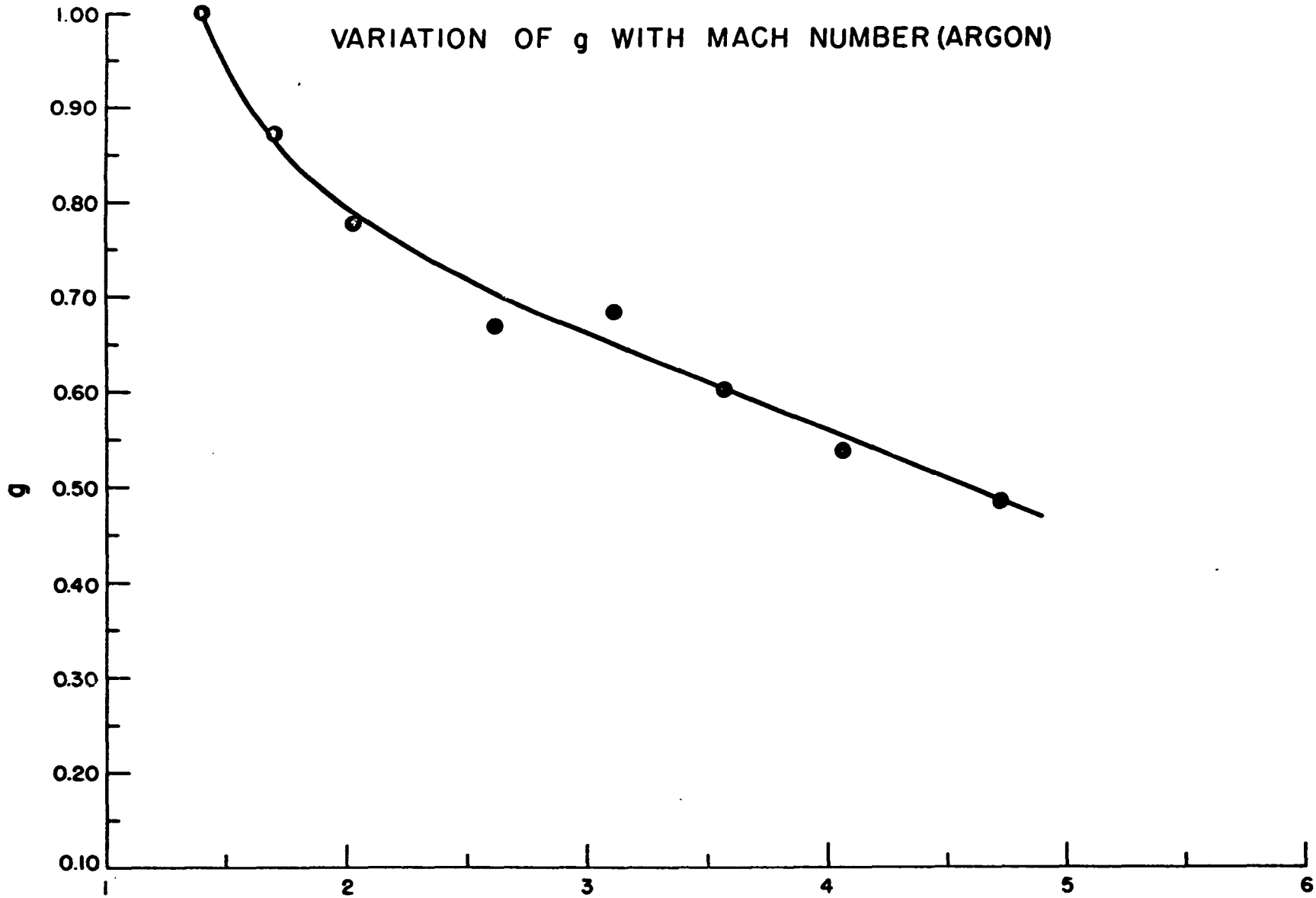
VARIATION OF g WITH MACH NUMBER (ARGON)
g
1.00
0.90
0.80
0.70
0.60
0.50
0.40
0.30
0.20
0.10
1
2
3
4
5
6
MACH NUMBER

FIG. 3

Figure 4

Variation of Reciprocal Shock Thickness (Mean Free Paths)

with Mach Number (Argon)

○ Table 2a) Present results

⊗ Table 2b)

□ Hansen and Hornig[4]

△ Talbot and Sherman[8]

1. Navier-Stokes theory[14], Lennard-Jones 6-12 potential

2. Bimodal theory[18]; a. (exp-rep) potential

b. Lennard-Jones 6-12 potential

c. modified Buckingham (exp-6) potential

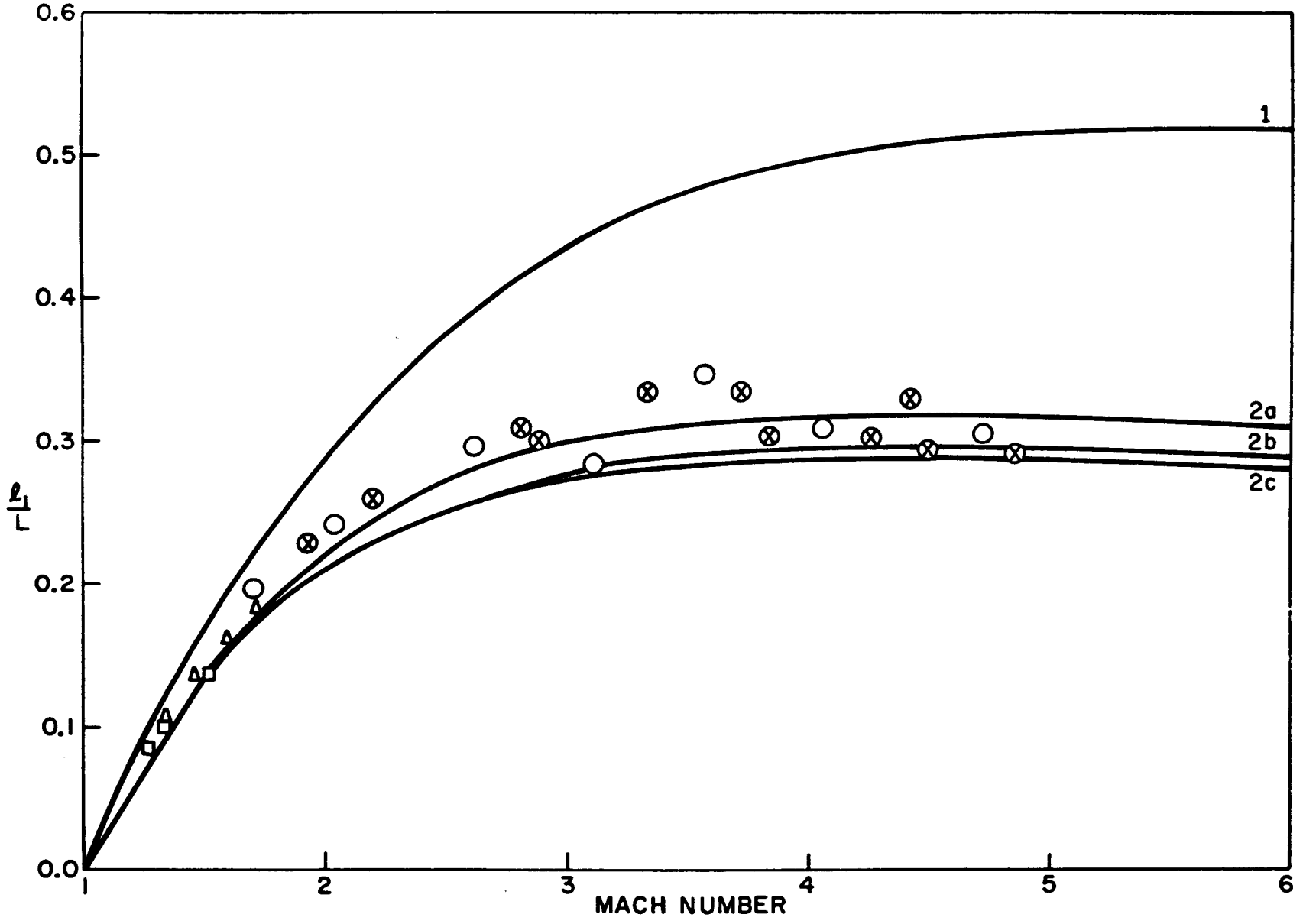


FIG. 4

Figure 5

Variation of Reciprocal Shock Thickness (Mean Free Paths)

with Mach Number (Nitrogen)

○ present results; △ Anderson and Hornig[3]; □ Greene and Hornig[2]

Theoretical curves calculated from the Navier-Stokes equations[19]

for bulk viscosity zero and 2/3 of shear viscosity.

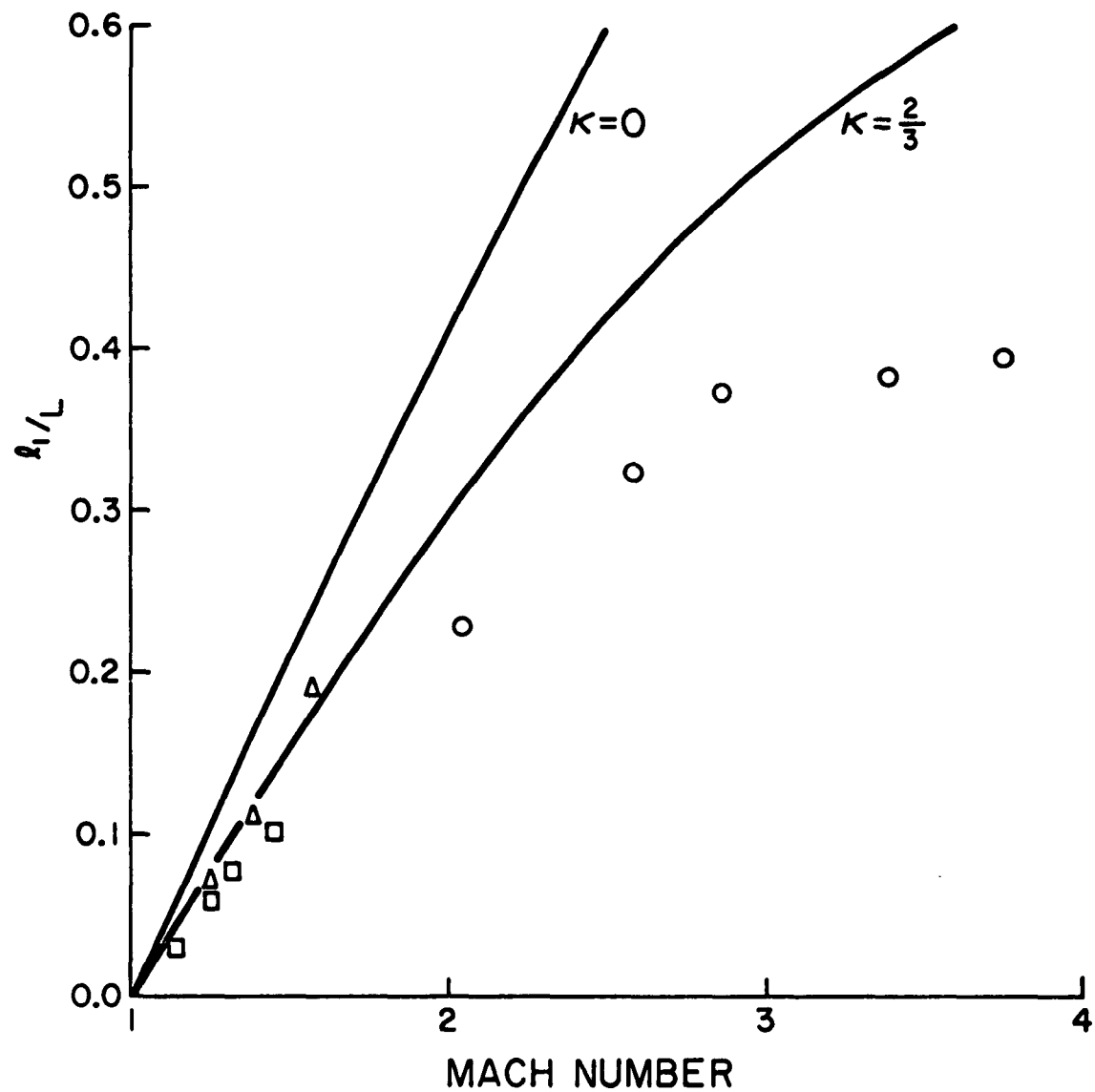
0.6
0.5
0.4
0.3
0.2
0.1
0.0
$\ell_1/L$
$\kappa=0$
$\kappa=\frac{2}{3}$
1
2
3
4
MACH NUMBER

FIG. 5